

## Shear Behavior of Concrete-Filled FRP tubes

Mohamed Fathy<sup>1</sup>, Ehab Khalil<sup>2</sup>, Tarek K. Hassan<sup>3</sup>, and Amr A. Abdelrahman<sup>4</sup>

<sup>1</sup>Graduate Student, Faculty of Eng., Ain Shams University, Cairo, Egypt

<sup>2</sup>Associate Professor, Construction Research Institute, National Water Research Center, Cairo, Egypt

<sup>3</sup>Associate Professor, Faculty of Eng., Ain Shams University, Cairo, Egypt

<sup>4</sup>Professor of Concrete Structures, Faculty of Eng., Ain Shams University, Cairo, Egypt

**ABSTRACT:** The main objective of this research is to describe the shear capacity of Concrete-Filled FRP Tubes (CFFT). A total of nine Glass FRP (GFRP) tubes were filled with concrete and tested as beams under a concentrated load at the mid span with various shear span-to-depth ratios ( $a/D$ ). Tested beams were divided into two main groups; the first group consisted of four tubes filled with plain concrete, while the second group consisted of five concrete filled tubes provided with extra longitudinal steel reinforcement. An elaborated Strut-and-Tie (S&T) model was adopted to model the shear behavior of CFFT beams. Geometry of the tension ties and compressive struts are established to present the tension fields in the external FRP shell and compression fields in the concrete core, respectively. The adopted model can closely simulate the internal force flow and predict the ultimate failure load.

### 1 INTRODUCTION

In the last decade, many concepts utilizing new construction materials are recognized. One of the most thriving concepts is the Concrete Filled FRP Tubes (CFFT). Researchers have attempted to extend available theories to predict the structural capacity of CFFT. ACI 440R-07 included many empirical expressions to predict the axial capacity of CFFT. Based on regression analysis of finite element results, with  $H/D$  ratio equal to two, the following empirical expression was proposed by Ahmed (2005):

$$f'_{cc} = f'c + (-0.2 fr^2 + 4.49 fr + 6.23) \quad (1)$$

where

$f'_{cc}$  = the confined concrete strength;

$f'c$  = the unconfined concrete strength;

$fr$  = the ultimate confining stress.

Recent attempts to address the shear behavior of CFFT in terms of ultimate concrete strength and shell properties were addressed by Seible et al. (1999). As a culmination for the recent researches four glass FRP tubes were tested to investigate the shear response of CFFT by Iftekhar (2004). Test results showed that the critical shear span-to-depth ratio ( $a/D$ ) for CFFT beams is much lower than one, which indicated that deep beams are more susceptible to shear failure than flexural failure. Furthermore, the test results of the tested deep beams resulted in higher flexural capacity than that theoretically calculated values using Bernoulli's beam theory (BBT), confirming that the BBT and the assumption of linear strain distribution are no longer valid for deep CFFT beams. Therefore, a new approach should be developed to analyze deep CFFT beams.

The primary objective of this research is to investigate the shear behavior of CFFT both experimentally and analytically and to attempt to develop an analytical model that can be used to predict the shear capacity of CFFT beams.

## 2 EXPERIMENTAL PROGRAM

A total of nine Glass FRP (GFRP) tubes were filled with concrete and tested as beams under a concentrated load at the mid span with various shear span-to-depth ratios ( $a/D$ ) in the experimental program. The tested beams were divided into two main groups; the first group consisted of four GFRP tubes filled with plain concrete, while the second consisted of five concrete filled GFRP tubes provided with extra longitudinal steel reinforcement. Table 1 summarizes the details of the beams properties used in this experimental program.

Two types of GFRP tubes were used in this program. All tubes of the first type (GFRP-1) have the same interior diameter which is equal to 200 mm with wall thicknesses equals to 6.7 mm. Tubes of the second type (GFRP-2) have an interior diameter of 300 mm with wall thickness equals to 7.3 mm. Table 2 provides detailed description of the tubes material including diameter, wall thickness and the mechanical properties of the GFRP tubes. To determine the compressive strength of the concrete core, three concrete cubes measuring 150 X 150 X 150 mm for each mix, were cast and cured in water then tested at the same day of testing their respective beams.

Table 1: Matrix for tested specimens

Beam ID	Diameter (D) mm	Span (L) mm	Shear span-to-depth ratio ( $a/D$ ) ----	Concrete strength at testing date MPa	Tube type	Reinforcement
<b>Group 01</b>						
B1	200	660	1.00	52	GRP-1	Plain
B2	200	860	1.50	48	GRP-1	Plain
B3	200	1060	2.00	41	GRP-1	Plain
B4a	200	660	1.00	52	GRP-1	Plain
B4b	200	460	0.50	52	GRP-1	Plain
<b>Group 02</b>						
B5a	200	660	1.00	40	GRP-1	3T16
B5b	200	460	0.50	40	GRP-1	3T16
B6	200	860	1.50	31	GRP-1	3T16
B7	300	860	1.00	28	GRP-2	3T16
B8	300	1010	1.25	31	GRP-2	4T16
B9	300	1430	1.95	31	GRP-2	5T16

Table 2: Mechanical properties of used GFRP tubes

Material	Internal diameter mm	Thickness of wall mm	Axial direction			Poisson's ratio ( $\mu$ )	Hoop direction	
			$f_u$ (ten.) (MPa)	$f_u$ (comp.) (MPa)	E (GPa)		$f_u$ (ten.) (MPa)	E (GPa)
GRP-1	200	6.7	66.3*	116.2*	7.2*	0.16*	187*	21.7*
GRP-2	300	6.9	62.6*	112*	7*	0.16*	238*	22*

\*Tested by Ahmed, (2005)

The used steel reinforcement was ribbed bars of grade 36/52. 16 mm diameter straight bars (with no hooks at the end) were used as main reinforcement (flexure reinforcement) in the longitudinal direction located at the bottom of the specimen.

### 2.1 Instrumentation and test setup

A mechanical dial gage was used to measure the mid-span deflection for all beams. Strain measurements were monitored using strain rosettes created by placing three electrical strain gages (placed in the diagonal, radial & longitudinal directions) at mid-height of the beam in the centre of the shear span. Each beam was further instrumented with electrical strain gages installed at the mid-span at the bottom surface of the specimens. Figure 1 shows a real view for the test setup while Figure 2 illustrates a typical schematic diagram for test setup.

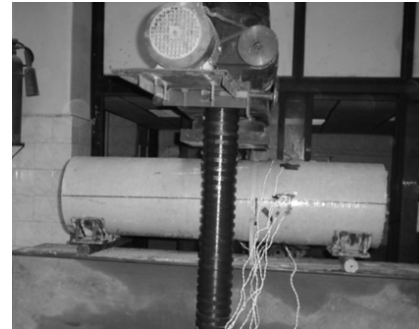


Figure 1: Real view for test setup

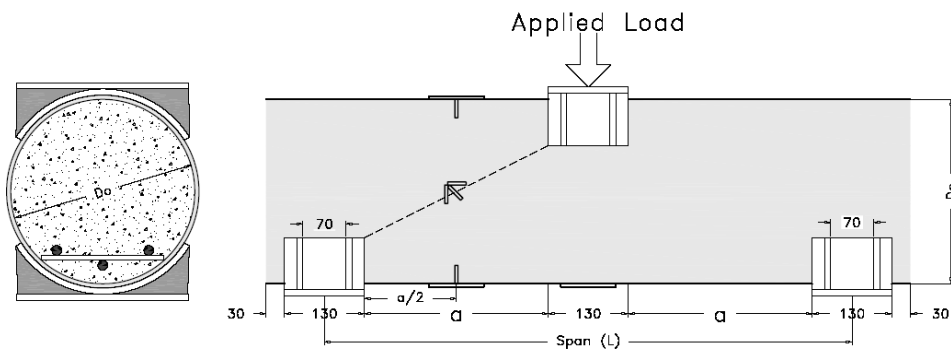


Figure 2: Typical schematic diagram for test setup

## 3 TEST RESULTS AND DISCUSSION

### 3.1 Failure Mechanism

All beams failed by rupture of the FRP tube in the extreme tension fibre except beams B5a, B5b and B4b, which exhibited classical shear failure. Figure 3 depicts typical flexural failure mode that was observed for most of the tested beams. Beams B4b and B5b exhibited pure shear failure, which was characterized by a sudden inclined shear crack associated with an audible noise. This was followed by a longitudinal crack at the bottom of the beam near the support; Figure 4 illustrates the crack pattern at shear failure. The cracks started and propagated too fast that caused a sudden loss in the beam stiffness.



Figure 3: Typical flexural failure mode of the tested specimens

Beam B5a experienced a combined flexure-shear failure. Figure 4-b shows two types of cracks occurred during loading. The first type was the inclined shear crack that appeared at approximately 76% of the ultimate capacity of the beam. In spite of shear cracks, the beam

sustained load increments until the second crack occurred and suddenly propagated from bottom to top. In this stage the beam reached its ultimate capacity.

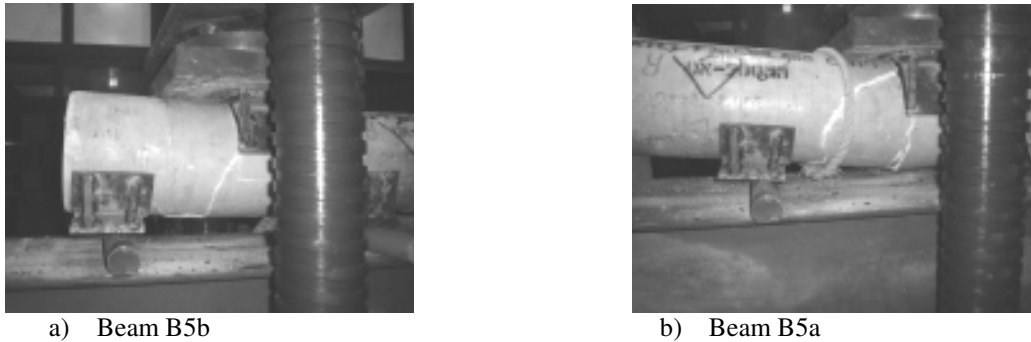


Figure 4: Typical crack pattern for shear failure

Table 3: Failure loads and maximum deflection at mid span for the tested specimens

Beam ID	B1	B2	B3	B4a	B4b	B5a	B5b	B6	B7	B8	B9
Failure load (KN)	150	90	85	160	255	500	700	350	600	715	490
Deflection (mm)	9.00	14.70	N.A.	13	N.A.	16.50	N.A.	17.32	14.00	18.75	18.00

### 3.2 Specimens Behavior

Figure 5 shows the relationship between the total applied load and mid-span deflection for plain specimens. Test observations and deflection measurements showed that the load-deflection response of plain specimens is almost linear until flexural cracks occurred followed by sudden loss of the beam stiffness up to failure. Conversely, reinforced concrete specimens showed significant strength and tangible rise in the stiffness compared to plain specimens. The load-deflection behaviour of reinforced beams is presented in Figure 6.

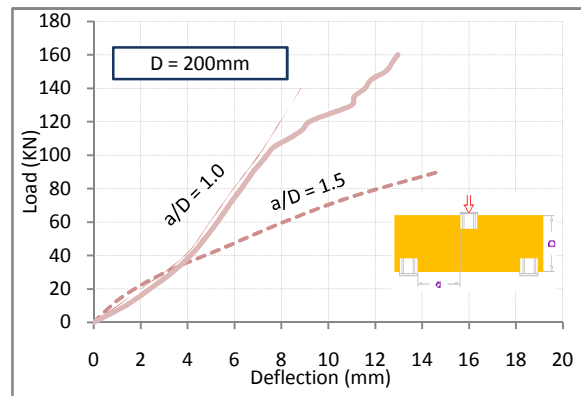


Figure 5: Load-deflection relationship for plain specimens

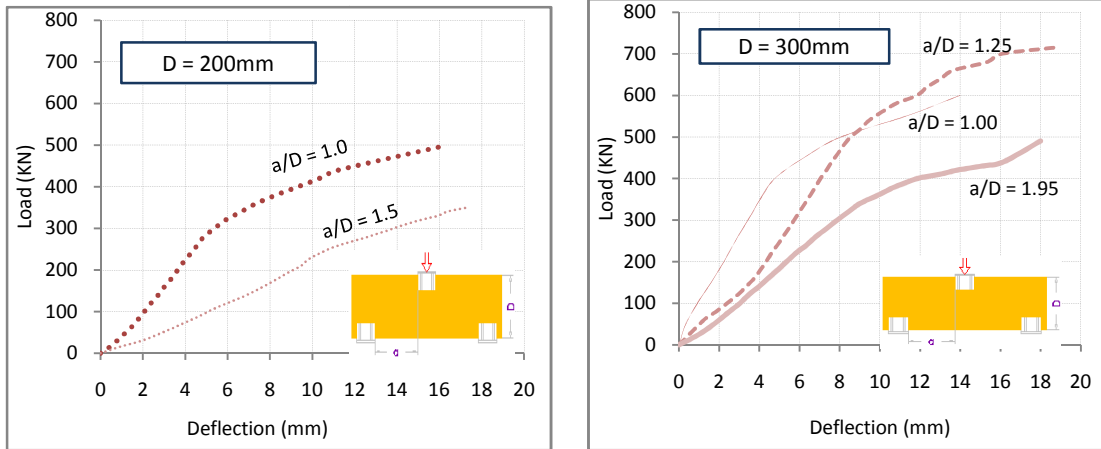


Figure 6: Load-Deflection relationship for reinforced specimens

### 3.3 Internal Stresses in GFRP Shell

The degree of nonlinearity of the induced stress in the tube can be experimentally measured in terms of strains. Figure 7 shows the measured longitudinal tensile strain due to bending at the most bottom fibres of the tested specimens. Figure 8 depicts the diagonal strain measurements at the mid height in centre of shear span. For plain specimens, the induced tensile stress in the longitudinal direction was linear and directly proportional to the load. The relationship between load and longitudinal strain of fibres in reinforced specimens can be idealized as a bilinear relationship. At the early loading stages, the behaviour is governed by the high modulus of elasticity of the steel reinforcement. At about 75% of the ultimate capacity of the beam, the steel reinforcement reached its yield strength. At this stage, additional loads are transferred to the GFRP shell. Consequently, the strain at this stage is controlled by the modulus of elasticity of the GFRP material, which is much smaller compared to that of the steel reinforcement. At the very early loading stages, load is carried totally by concrete without any contribution from the shell. Test results showed that diagonal strain gages, installed at the middle of the shear span, started to record induced strains in the shell (Figure 8) at about 30% of the ultimate beam capacity.

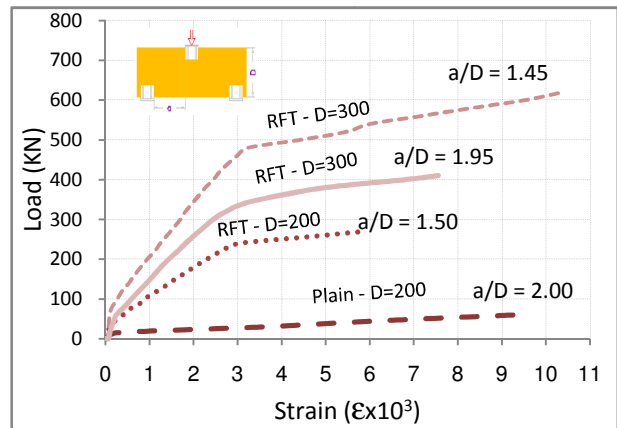


Figure 7: Load-flexure strain relationship

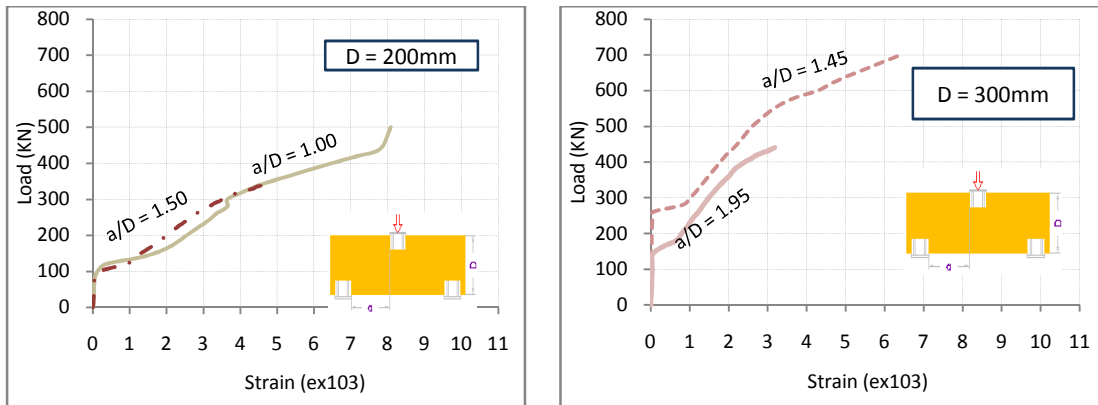


Figure 6: Load-Diagonal strain relationship for reinforced specimens

#### 4 STRUT AND TIE MODEL

Geometry of the tension ties and compressive struts are established to present the state of stresses in the external FRP shell and concrete core while keeping the angle of inclination for principal tie/strut within reasonable limits. Figure 9 illustrates the geometry of the proposed strut and tie model. The main assumptions are:

- Shear strength of the GFRP shell in both longitudinal and transverse directions is very small compared to the tensile strength and can be ignored.
- Tensile strength of the GFRP shell in any inclined direction can be predicted based on principal stresses circle (Mohr's circle) as shown in Figure 10, considering the hoop strength as the maximum tensile strength of the shell, according to equation (2).

$$F_p = 0.5(F_r + F_t) + 0.5(F_r - F_t)\text{Cos}[2(90 - \theta)] \quad (2)$$

where:

$F_p$  = Tensile strength of GFRP shell in a particular inclined direction.

$F_t$  = Tensile strength of the GFRP shell in the longitudinal direction.

$F_r$  = Tensile strength of the GFRP shell in the hoop direction.

$\theta$  = inclination angle of the inclined tie to the longitudinal axis of the beam

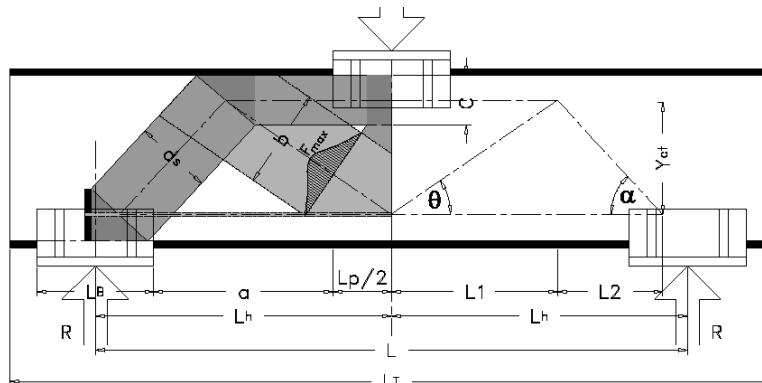


Figure 7: Strut-and-tie model dimensions and members sizes

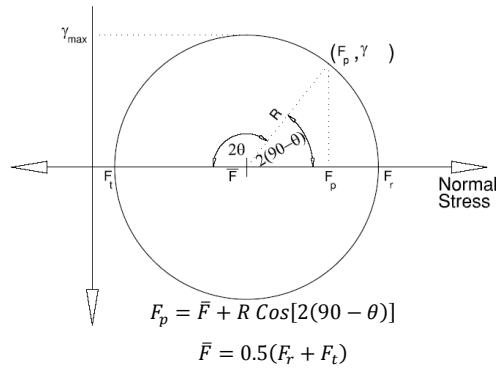


Figure 8: Mohr's circle used to predict the tensile strength of GFRP shell in a particular inclined direction

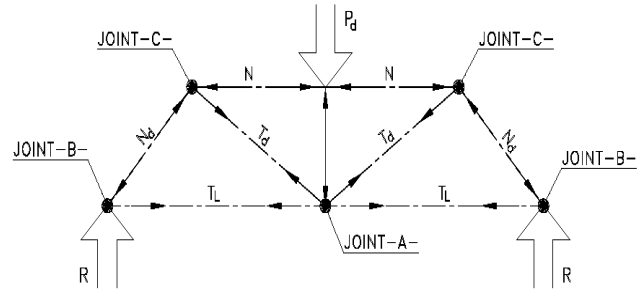


Figure 9: Free body diagram showing the induced truss forces due to applied concentrated dummy load at mid span

#### 4.1 Members dimensioning

The effective width of the inclined tie was calculated based on the geometry of the beam shown in Figure 9 and given by equation (3), while the cross sectional area of the inclined tie was calculated as proposed in equation (4).

$$b = \frac{D}{\cos(\theta)} \quad (3)$$

$$A_{dt} = l \times t \times \eta \quad (4)$$

where:

$b$  = width of the inclined tie;

$D$  = Pipe Diameter;

$A_{dt}$  = Effective area of inclined tie;

$l$  = Circumference of the inclined ellipse  $\cong \pi \frac{(D+b)}{2}$ ;

$t$  = Pipe thickness;

$\eta$  = Correction factor to account for interference between members = 0.50.

In a similar way, the width of the inclined strut is given in Equation (5). For practical applications, the effective out of plan width of the strut ( $d_s$ ) can be taken equal to the effective out of plan width of the bearing plate at the support point. Accordingly, the cross sectional area of the inclined tie was calculated as expressed in equation (6).

$$d_s = \frac{l_B}{2 \sin(\alpha)} \quad (5)$$

$$A_{ds} = d_s \times b_s \quad (6)$$

where:

$d_s$  = width of the inclined strut;

$l_B$  = length of the bearing plate at support point;

$\alpha$  = Inclination angle of the strut to the horizontal direction;

$b_s$  = Effective out of plan width.

The ultimate resistance of the inclined tie and inclined strut were calculated as given in Equations (7) and (8) respectively. These Equations were driven based on the calculated member's dimensions.

$$T_{dR} = A_{dt} \times F_p \times \zeta \quad (7)$$

$$N_{dR} = A_{ds} \times F_c \quad (8)$$

where:

$T_{dR}$  = Ultimate resistance of the inclined tie;

- $F_p$  = Tensile strength of GFRP shell in the direction of the inclined angle as calculated using equation 2.  
 $\zeta$  = Correction factor to account for nonlinear stress distribution = 0.70  
 $N_{dR}$  = Ultimate resistance of the inclined strut (Force)  
 $F_c$  = equivalent constant stress = 0.85  $f_c'$

#### 4.2 Prediction of failure load

The free body diagram given in Figure 11 shows the induced forces in each member due to applied dummy load ( $P_d$ ). The factor of safety for each member is defined as the ratio between the ultimate resistances (as calculated in the previous section) and the induced forces of that member (as calculated from the free body diagram). The truss element that has the weakest capacity compared to the induced internal force will govern the overall failure mode of the beam. Accordingly, the magnitude of failure load can be calculated based on equation (9).

$$P_{ultimate} = P_d \times FOS_{least} \quad (9)$$

where:

- $P_{ultimate}$  = Ultimate concentrated load could be resisted by the beam at the mid-span  
 $P_d$  = Dummy concentrated load applied at the mid-span of the beam  
 $FOS_{least}$  = Least factor of safety for the members.

#### 4.3 Prediction of the inclination angle of principal tie ( $\theta$ )

In the adopted strut-and-tie model, the inclined tie has two main roles. First, is to enhance the bending capacity of the beam (i.e. longitudinal component of the induced force in the tie). Second, is to resist the applied shear force after degradation of shear capacity of the concrete core due to cracking (i.e. transverse component of the induced force in the tie). Accordingly, both of bending and shear capacities of CFFT beam are dependent on the angle of inclination of the principal tie ( $\theta$ ). In order to predict the most reliable  $\theta$ , it is assumed that  $\lambda$  is constant. In which the ratio  $\lambda = \frac{L_1}{L_h}$  where  $L_1$  is the horizontal projection of the tie and  $L_h$  is half the beam span. In the current study, the adopted strut-and-tie model was used to calibrate the values of  $\lambda$  based on the results obtained from the experimental program. The average values for  $\lambda$  for the tested plain and reinforced specimens were 0.55 and 0.30, respectively. Figures 12 and 13 depict the comparison between the experimental failure loads and the predicted failure loads using the adopted strut-and-tie for reinforced and plain specimens, respectively.

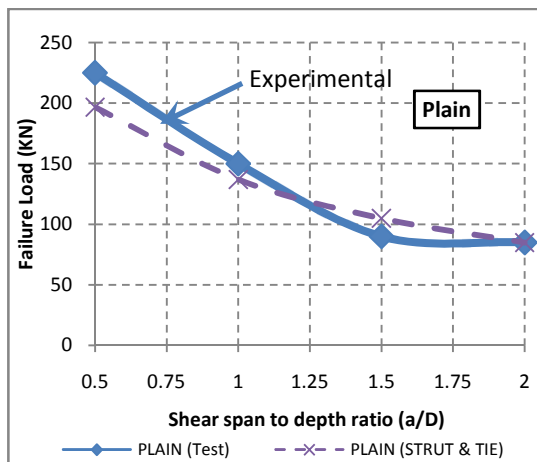


Figure 10: : Load VS (a/D) for plain specimens

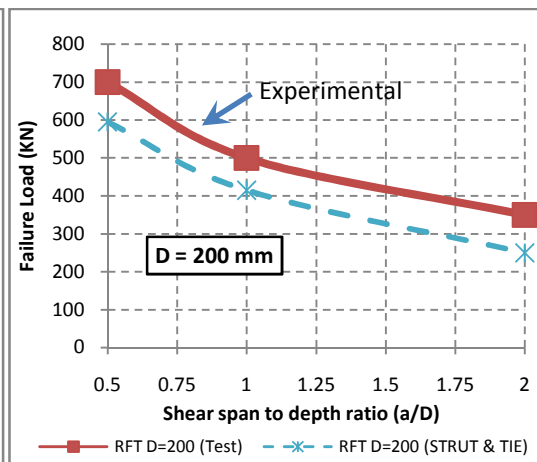


Figure 11: Load VS (a/D) for reinforced specimens

## 5 CONCLUSIONS

The presented research verified the potential of concrete-filled GFRP tubes as structural members with significant shear strength. Based on the experimental and the analytical studies, the following conclusions may be drawn:

- CFFT beams behave linearly till failure. The expected failure mode is rupture of the tube, rather than diagonal tension.
- Plain CFFT beams experience brittle failure, while reinforced CFFT beams experience ductile failure.
- Bernouli's beam theory is not valid for deep CFFT beams.
- The proposed strut and tie model can accurately be used to predict the shear capacity of CFFT.

## 6 REFERENCES

- Ahmed, Amgad, (2005) "Behavior of FRP filled-tube concrete columns under vertical loads" *PhD Thesis, Faculty of engineering, Ain Shams University, Egypt.*
- Ahmed, Iftekhhar, (2004) "Shear response and bending fatigue behavior of concrete-filled fiber reinforced polymer tubes," *PhD Thesis, Graduate Faculty of North Carolina State University.*
- Seible, F., et al. (1999) "Kings Stormwater Channel and I-5/Gilman Bridge," *Structural Engineering International, Journal of the International Association for Bridge and Structural Engineering, V. 9, No. 4, pp. 250-253.*